Dynamics of Radially Expanding Liquid Sheets

Nayanika Majumdar and Mahesh S. Tirumkudulu[*]

Department of Chemical Engineering, Indian Institute of Technology Bombay, Powai, Mumbai 400076, India

The process of atomization often involves ejecting thin liquid sheets at high speeds from a nozzle that causes the sheet to flap violently and break up into fine droplets. The flapping of the liquid sheet has long been attributed to the sheet's interaction with the surrounding gas phase. Here, we present experimental evidence to the contrary and show that the flapping is caused by the thinning of the liquid sheet as it spreads out from the nozzle exit. The measured growth rates of the waves agree remarkably well with the predictions of a recent theory that accounts for the sheet's thinning but ignores aerodynamic interactions. We anticipate these results to not only lead to more accurate predictions of the final drop-size distribution but also enable more efficient designs of atomizers.

Atomization is the process of transition of a compact liquid mass to dispersed drops, and it involves a transient stage of unstable liquid jets or sheets [1]. The process is important industrially, with applications in areas as diverse as combustion [2], food and pharmaceuticals [3], agriculture [4,5], and fire protection [4]. One of the most common techniques to atomize liquid is to produce high-speed, thin liquid sheets either by impinging a liquid jet on an inclined surface, such as in a floodjet nozzle, or by ejecting the liquid through a thin slit, such as in a fan spray nozzle [1,6]. In either case, the sheet expands radially outward from the point of impingement or the nozzle exit, flaps violently, and atomizes within a short distance from the tip of the nozzle. While the final stages of sheet breakup are complex, involving highly deformed interfaces and turbulent flows, the first estimate of the drop-size distribution is obtained from the linear stability analysis of the thin moving sheet [6].

To this end, Squire [7] was the first to analyze the stability by considering the inviscid flow of a two-dimensional film of a *constant* thickness in an inviscid gas phase. It was shown that the oscillations of the sheet are a combination of varicose(symmetric) and sinuous(antisymmetric) modes. The analysis focused on the latter since the degree of instability for long waves of thin water sheets moving in air is much larger for the sinuous mode compared to the varicose mode. The instability is caused by the inertia of the liquid while surface tension (σ) stabilizes it, resulting in one of the necessary conditions for instability, $\mathrm{We}_h \equiv \rho_l U^2 h/\sigma > 2$. Here, We_h is the Weber number calculated with respect to the film thickness (h), U is the speed of the moving liquid sheet, and ρ_l is the density of the liquid phase.

The temporal growth rate of the sinuous wave can be estimated via a simple scaling analysis [8]. In the reference frame of the moving sheet, a small sinuous perturbation of amplitude y and wavelength λ, surrounded by a gas phase

of density, ρ_g, results in a pressure difference of $\rho_g U^2 y/\lambda$ between the peak and the trough of the deformed sheet. This pressure difference causes the initial perturbation to grow, thereby accelerating the trough and the peak in opposite directions. Equating the mass times acceleration of a section of trough (or peak), $\rho_l h \ddot{y}$, to the pressure difference, results in the scaling for the growth rate of a sinuous wave, $U\sqrt{(\rho_g/\rho_l)(1/h\lambda)}$, with the dot representing the time derivative. Thus, the growth of the instability is proportional to the square root of the ratio of the fluid densities and is inversely proportional to the square root of the thickness. In absence of a gas phase, the constant thickness sheet is always stable.

The aforementioned analysis of Squire [7] has been used for more than seven decades to determine the stability of not only constant thickness sheets but also for radially expanding sheets, where the thickness decreases inversely with the radial distance (r) from the nozzle exit [8–19]. In fact, Squire [7] himself analyzed the atomization of radially expanding, conical sheets using this theory by stating that, "It is not practicable to investigate the stability of a conical film of variable thickness, and it is considered that most of the important features are included in the two-dimensional problem." However, problems with assuming a constant thickness film for a radially thinning sheet have been recognized, but progress has been prevented by the "theoretical difficulties" [10] of accounting for a thinning geometry. As a result, even recent studies have adopted the "locally parallel" assumption on the grounds that the slope of thickness scales as $1/r^2$, which becomes vanishingly small a few jet diameters away from the jet. Consequently, the correction is considered to be only a second order effect, thereby permitting a constant thickness assumption [15–18].

The aforementioned difficulty of accounting theoretically for the thinning geometry was overcome recently in a
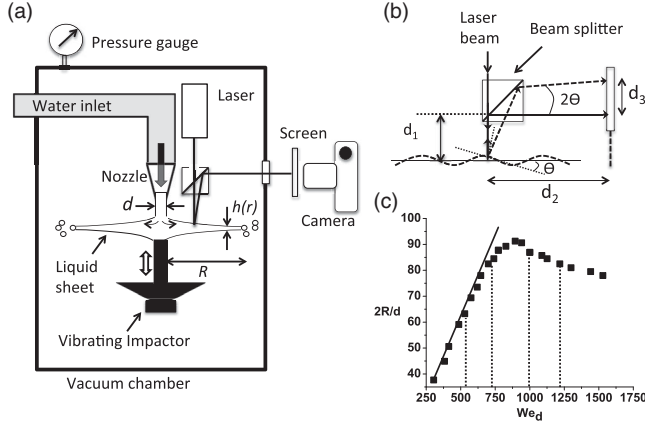
FIG. 1. (a) Experimental set-up for generating radially expanding liquid sheet. Sinusoidal motion of the vibrating impactor generates sinuous waves that are convected radially outward. (b) Surface inclination angle, θ, of the surface waves is related to the displacement, d_3, of the laser spot on the screen. (c) Measured dimensionless sheet radius versus We_d in the absence of forcing and at atmospheric pressure. The solid line represents, $2R/d = \mathrm{We}_d/8$. The vertical dotted lines represent We_d at which the spatial growth rates of sinuous waves were determined.

new study [20], which showed that sinuous waves grow spatially, even in the absence of the surrounding gas phase. The growth was attributed to the thinning of the sheet although aerodynamic interactions were expected to dominate at large liquid speeds [21,22]. In this Letter, we present conclusive experimental evidence to the contrary and show that, in the *linear* regime and for up to atmospheric pressures, the dynamics of a radially expanding sheet are entirely dominated by its thinning in the radial direction, even at very large liquid speeds, with negligible influence of the surrounding gas phase.

The experimental setup, illustrated in Fig. 1, is comprised of a laminar jet emanating from a vertical converging borosilicate glass nozzle of exit jet diameter (d) 2.5 mm and impacting on a solid stainless cylinder of diameter 9 mm placed below it. On impact, the liquid jet spreads out radially into a thin liquid sheet [18,23].

Past studies have shown that the sheet thickness varies inversely with the radial distance (r) from the impingement point, $h = d^2/8r$, which is obtained by balancing the mass of the incoming liquid from the jet, $\pi d^2 U/4$, with the mass of the outgoing liquid at a radial location r far from the point of impingement, $2\pi r U h$ [24–26]. In the absence of any disturbance, a balance of the momentum pushing the liquid out at the sheet's edge, $\rho_l U^2 2\pi R h$, against the surface tension force preventing the expansion, $2\sigma 2\pi R$, gives the diameter of the sheet, $2R/d = \rho_l U^2 d/8\sigma \equiv \mathrm{We}_d/8$ [25]. At low $\mathrm{We}_d < 700$, termed as the *smooth* regime, the sheet surface remains smooth, and the sheet radius increases linearly with We_d, in agreement with the predictions of the simple momentum balance equation [Fig. 1(c)]. However, as We_d is increased further, the sheet

increasingly becomes disturbed, and it flaps akin to a flag. Consequently, the sheet radius reduces with increasing We_d in the *flapping* regime, which has been attributed to the aerodynamic interactions [9].

The surface waves on the liquid sheet were determined via an optical arrangement comprised of a diode laser and a cube beam splitter fixed vertically below it [Fig. 1(b)]. This arrangement was placed on a motorized traverse, so as to scan deflections along the radial direction. The technique is very sensitive to surface perturbations, and it has been shown to measure surface wave amplitudes as low as 10 nm [27,28]. Previous experiments have shown that the amplitude of the varicose waves (or thickness modulations) are small, except close to the edge, indicating that the surface waves are solely due to the sinuous mode of sheet deformation [21,29,30]. The reflected laser beam from the wavy surface of the liquid sheet is projected onto a graduated screen, and the position of the laser spot is recorded in time. Sinuous waves of a required frequency were generated by placing the vertical impactor on a vibrating stage. The entire setup was placed inside a vacuum chamber, enabling experiments under subatmospheric pressure conditions. As the waves move past a fixed point on the sheet, the reflected laser spot oscillates on the screen. The surface inclination angle of the liquid sheet with respect to the horizontal, θ, is related to the displacement of the laser spot (d_3) by $\tan(2\theta) = d_3/(d_1 + d_2)$, where d_1 and d_2 are defined in Fig. 1(b). A fast Fourier transformation of the time series data gives the frequency and the amplitude of the (oscillating) inclination angle of the dominant waves. The maximum inclination angle was less than $4°$ in all cases, indicating that the deformation was in the linear regime (see Supplemental Material [31]).

The measured amplitudes of the surface inclination angle were compared with the predictions of the new theory that accounts for the thinning of the radially expanding liquid sheet but ignores aerodynamic interactions [20]. The main result of the analysis can be understood via a scaling analysis that balances the centrifugal force exerted by liquid flowing in a curved section of the sheet with the line tension resisting it,

$$-\rho_l U^2 h(r)\frac{\partial^2 F_+}{\partial r^2} + 2\sigma\nabla_r^2 F_+ \sim \rho_l h(r)\frac{\partial}{\partial t}\left(\frac{\partial F_+}{\partial t} + U\frac{\partial F_+}{\partial r}\right),$$
(1)

Here, F_+ is the centerline position of the sheet and is a function of r and time, t. Rendering h and r dimensionless with characteristic thickness, h_0, and radial distance, $r_0(=d^2/8h_0)$, respectively, along with $\bar{F}_+ = F_+/h_0$ and $\bar{t} = tU/r_0$ gives,

$$\frac{\partial^2 \bar{F}_+}{\partial \bar{r}^2}\left(\frac{2\bar{r}}{\mathrm{We}_h} - 1\right) + \frac{\partial \bar{F}_+}{\partial \bar{r}}\left(\frac{2}{\mathrm{We}_h}\right) \sim \frac{\partial^2 \bar{F}_+}{\partial \bar{t}^2} + \frac{\partial^2 \bar{F}_+}{\partial \bar{t}\partial \bar{r}} \quad (2)$$

where, We_h is defined with respect to h_0. Note that $2\bar{r} < We_h$ everywhere except at the edge of the sheet, where $2\bar{r} = We_h$, implying that the coefficient of the first term in (2) goes to zero at the edge. For a sheet that vibrates at a fixed frequency, the spatial growth of the corresponding wave is determined by setting, $\bar{F}_+ = \bar{S}(\bar{r})e^{i\bar{\omega}\bar{t}}$, and solving, $[(2\bar{r}/We_h) - 1]d^2\bar{S}/d\bar{r}^2 + \omega^2\bar{S} \sim 0$. Here, $\bar{\omega} \equiv \omega R/U$ is the dimensionless frequency, and a small slope $(d\bar{S}/dr \ll 1)$ is assumed. The analytical solution is a Bessel function of the first order that diverges at the edge of the sheet irrespective of $\bar{\omega}$, $\bar{S} \to (1 - 2\bar{r}/We_h)^{-1/2}$ (see Supplemental Material [31]).

A more exact equation describing the dynamics is derived from a regular perturbation analysis $(h_0/r_0 \ll 1)$ of the inviscid flow problem for a thin, radially expanding sheet [20],

$$\frac{\partial^2 \bar{F}_+}{\partial \bar{r}^2}\left[\frac{2\bar{r}}{We_h} - 1\right] + \frac{\partial \bar{F}_+}{\partial \bar{r}}\left[\frac{2}{We_h} + \frac{1}{\bar{r}}\right]$$
$$= \frac{\partial^2 \bar{F}_+}{\partial \bar{t}^2} - \frac{\partial \bar{F}_+}{\partial \bar{t}}\left[\frac{1}{\bar{r}}\right] + 2\frac{\partial^2 \bar{F}_+}{\partial \bar{r}\partial \bar{t}}. \tag{3}$$

Substituting for $\bar{F}_+$ in (3) and solving for $\bar{S}$ with the conditions of zero slope and a small but finite perturbation $(\bar{S}_0)$ close to the impingement point [20,21], shows that wave amplitude diverges at the edge of the sheet, just as in the scaling analysis, but now more quickly, $\bar{S} \to (1 - 2\bar{r}/We_h)^{-1}$ [20]. The resulting differential equation can be rescaled so that the results for varying $X \equiv \bar{r}/We_h$ collapse onto a single master curve for a fixed $N \equiv \bar{\omega}We_h$,

$$\frac{d^2(\bar{S}/\bar{S}_0)}{dX^2}[2X - 1] + \frac{d(\bar{S}/\bar{S}_0)}{dX}\left[2(1 - iN) + \frac{1}{X}\right]$$
$$+ \left(\frac{\bar{S}}{\bar{S}_0}\right)\left[N^2 + \frac{iN}{X}\right] = 0. \tag{4}$$

The slope of the wave, $\tan\theta$, is obtained by taking the derivative of $\bar{F}_+$ with respect to $\bar{r}$ and retaining the real terms in the resulting expression. Given the complex nature of flow at the impingement point, it is not possible to determine experimentally, the amplitude of the perturbation induced by the oscillating impactor at the impingement point. Therefore, the value of $\bar{S}_0$ was chosen such that the theoretical curve passes through the first data point for each frequency. This is equivalent to inserting the measured perturbation of the first data point into the model and then predicting the rest of the spatial growth. Thus, there are no fitting parameters in the solution procedure. Further details are given in the Supplemental Material [31].

Figure 2 shows the spatial growth of the sinuous waves for the smooth regime ($We_d = 550$ and 700) and for varying forcing frequencies. The plot also includes spatial growth at 0.6 atm to determine the influence of the surrounding gas
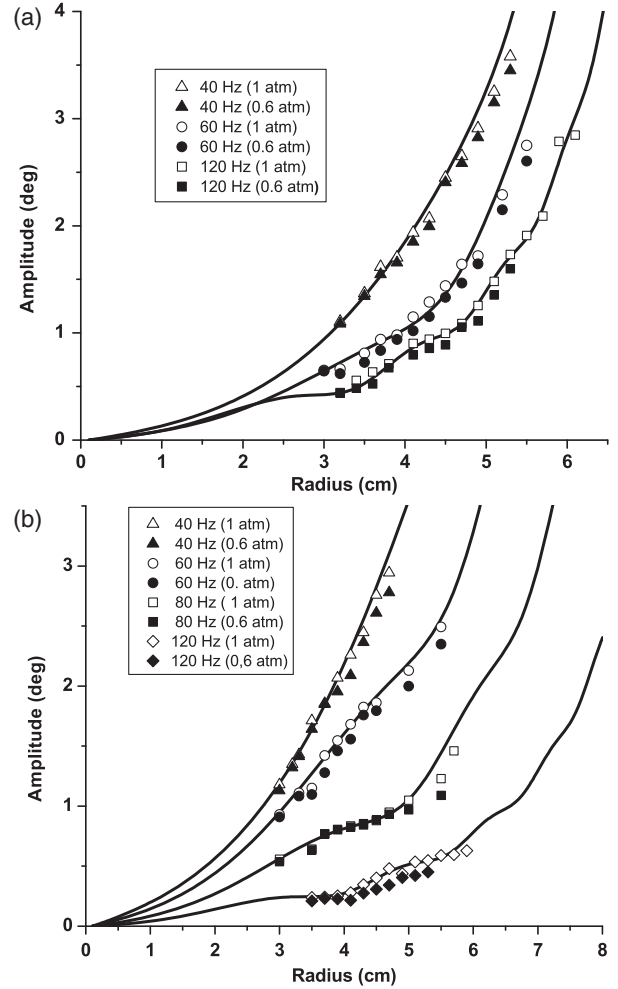
FIG. 2. Measured amplitude of surface inclination angle at different radial locations is compared with predictions (lines, (3)) in the smooth regime for a range of forcing frequencies and at 1 and 0.6 atm, (a) $We_d = 550$ and (b) $We_d = 700$.

phase on the spatial growth. Clearly, there is an excellent agreement between the prediction and the measurements at both pressure conditions. While the amplitudes all diverge at the edge of the sheet irrespective of the forcing frequency, lower frequencies show high growth rates closer to the impingement point. This is captured accurately by the model. The data at the subatmospheric pressure are only marginally lower in some cases but follow the predicted profiles closely, which clearly shows that gas phase inertia has a negligible impact, and the growth is on account of the thinning effect. The error bars (not shown) are within $\pm5\%$ of the mean values for all cases.

Figure 3 presents the spatial growth for $We_d = 975$ and 1200, which correspond to the *flapping* regime. There is an excellent agreement between the measurements and the predictions at $We_d = 975$ for all three frequencies and at both ambient pressures. At the highest We_d, experiments could not be performed at subatmospheric pressure since the fine drops ejected from the edge of the sheet led to
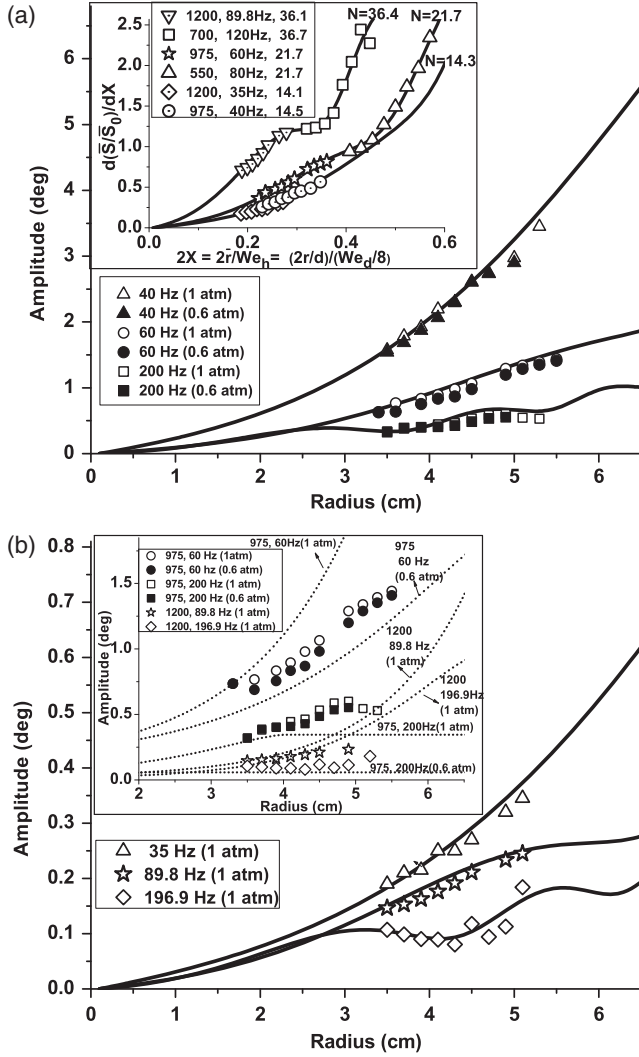
FIG. 3. Measured amplitude of surface inclination angle at different radial locations is compared with predictions (lines) in the flapping regime for a range of disturbance frequencies, (a) $We_d = 975$ at 1 and 0.6 atm. The inset shows the collapse of three sets of measurements for fixed N across all We_d and varying $\bar{\omega}$ (legend: We_d, frequency, N). The solid lines are theoretical predictions (4) for a fixed N, and (b) $We_d = 1200$ at 1 atm. Note that the frequencies at $We_d = 1200$ correspond to the highest natural modes in the system. The inset compares measurements with predictions of the aerodynamic theory (dotted lines) for $We_d = 975$ and 1200 (see Supplemental Material for details [31]).

significant water condensation on the beam splitter. The same problem was encountered during forcing under atmospheric conditions, as it led to a dense spray. Since the sheet flapped significantly even in the absence of forcing, we obtained the growth rate for frequencies of the three highest natural modes present in the system at atmospheric pressure. These modes are attributed to the disturbances in the system and may be caused by the pump, the vibrations induced by flow in the piping and/or the

impactor assembly. Importantly, the amplitude of the disturbances increased with flow rate enabling reliable measurements at high We_d. The predictions of the spatial growth match remarkably well with the measurements and capture the variation in spatial growth with frequency. These results clearly show that the growth of the sinuous waves are completely determined by the thinning of the radially expanding sheet even at a very high We_d. The inset of Fig. 3(a) shows the collapse of the data in the rescaled coordinates across varying We_d and $\bar{\omega}$ for three different values of N, demonstrating the existence of a master curve for a fixed N. These results reinforce the claim that the growth of the sinuous waves for the range of experimental conditions tested here, whether in the smooth regime or in the flapping regime, is controlled by the thinning of the liquid sheet and not by aerodynamic interactions.

A corollary to these findings is that the decrease in sheet diameter with increasing We_d in the flapping regime is not due to aerodynamic interactions, as previously proposed, but is a function of the disturbances present in the system. Thus, the transition from the smooth to the flapping regimes may be delayed by reducing the intensity of such disturbances. These conclusions are supported by the experiments of Crapper and Dombrowski [33] on fan spray nozzles in the flapping regime, who showed that the dominant frequencies of a flapping sheet and the subsequent drop size distribution are significantly influenced by the resonance of the apparatus, indicating that different experimental rigs can cause a spray nozzle to produce different drop-size spectra. Experiments on air-assisted nozzles, wherein a liquid sheet is sandwiched between two sheets of high-speed air to enhance atomization, show that the effect of introducing air in the nozzle is similar to the effect of inducing forced vibrations on the nozzle jaws. Thus, for each air flow rate, there is a specific vibration frequency for the nozzle [30].

In sharp contrast to the above results, the aerodynamic theory [7] predicts nonzero spatial growth rates only up to a critical radius, whose value increases with We_d but decreases with forcing frequency (see Supplemental Material for a detailed comparison [31]). Consequently, the growth rates are negligible for $We_d = 550$ and 700 for all frequencies tested in the experiments. At $We_d = 975$, the measured amplitudes are higher at 60 Hz, while they are lower than the predictions at 200 Hz [inset of Fig. 3(b)]. Further, the aerodynamic theory predicts a stable sheet beyond 4 cm at 200 Hz, while measurements show a growing sinuous mode. More importantly, the predicted amplitude decreases substantially at the lower pressure (0.6 atm), which is not observed in the experiments. At the highest We_d, the predicted amplitudes are much higher than the measurements. These results point to the general failure of the aerodynamic theory in capturing even the most basic trends observed in the experiments. Recent simulations of thin, *constant* thickness sheets [34,35] show

that the growth rates predicted by the aerodynamic theory are significantly higher, by more than a factor of two, than the measurements. They show that the presence of a thin gas boundary layer next to the liquid-gas interface significantly dampens the growth rate. Consequently, the influence of the aerodynamic interactions on the growth of sinuous waves should be smaller than that predicted by the aerodynamic theory.

With a more accurate description of the dynamics of radially expanding liquid sheets, it should now be possible to obtain a more accurate prediction of the final drop-size distribution. These findings are especially relevant to industrial nozzles, such as the fan spray and the floodjet nozzles, where the sheet thickness reduces with distance from the nozzle tip. The growth of the sinuous waves would be dominated by the thinning effect in such cases [22]. As the sinuous waves grow spatially, the increasing oscillations of the liquid sheet make them susceptible to the Rayleigh-Taylor type of instability [36], which will set the radius of the undulating sheet. A thin liquid sheet accelerated perpendicular to itself breaks into droplets, whose average radius scales as $\sim (\sigma h/\rho_l |a|)^{1/3}$, where a is the acceleration imparted by the spatially growing sinuous wave and is given by the right-hand side of (3). Thus, increasing a by increasing forcing amplitude, liquid speed, and/or forcing frequency will lead to smaller droplets. Such strategies based on model predictions should lead to better designs of nozzles for control on the final drop-size distribution.

[*]mahesh@che.iitb.ac.in

[1] A. H. Lefebvre and V. G. McDonell, *Atomization and Sprays*, 2nd ed. (CRC Press, Boca Raton, 2017).

[2] A. H. Lefebvre, Atom. Sprays **10**, 251 (2000).

[3] K. Masters, *Spray Drying*, 2nd ed. (John Wiley, New York, 1976).

[4] G. E. McCreery and C. M. Stoots, Int. J. Multiphase Flow **3**, 431 (1995).

[5] G. J. Dorr, A. J. Hewitt, S. W. Adkins, J. Hanan, H. Zhang, and B. Noller, Crop protection **53**, 109 (2013).

[6] *Handbook of Atomization and Sprays*, edited by N. Ashgriz, 1st ed. (Springer, New York, 2011).

[7] H. Squire, Br. J. Appl. Phys. **4**, 167 (1953).

[8] E. Villermaux, Annu. Rev. Fluid Mech. **39**, 419 (2007).

[9] J. Huang, J. Fluid Mech. **43**, 305 (1970).

[10] G. Crapper, N. Dombrowski, and G. Pyott, Proc. R. Soc. A **342**, 209 (1975).

[11] D. Weihs, J. Fluid Mech. **87**, 289 (1978).

[12] E. A. Ibrahim and A. J. Przekwas, Phys. Fluids **3**, 2981 (1991).

[13] W. Sirignano and C. Mehring, Prog. Energy Combust. Sci. **26**, 609 (2000).

[14] C. Clanet and E. Villermaux, J. Fluid Mech. **462**, 307 (2002).

[15] E. Villermaux and C. Clanet, J. Fluid Mech. **462**, 341 (2002).

[16] S. P. Lin, *Breakup of Liquid Sheets and Jets*, 1st ed. (Cambridge University Press, Cambridge, 2003).

[17] S. P. Lin and W. Y. Jiang, Phys. Fluids **15**, 1745 (2003).

[18] N. Bremond, C. Clanet, and E. Villermaux, J. Fluid Mech. **585**, 421 (2007).

[19] M. Altimira, A. Rivas, J. C. Ramos, and R. Anton, Atom. Sprays **22**, 733 (2012).

[20] M. Tirumkudulu and M. Paramati, Phys. Fluids **25**, 102107 (2013).

[21] M. Paramati, M. Tirumkudulu, and P. Schmid, J. Fluid Mech. **770**, 398 (2015).

[22] N. Majumdar and M. S. Tirumkudulu, Phys. Fluids **28**, 052101 (2016).

[23] G. Taylor, Proc. R. Soc. A **253**, 313 (1959).

[24] F. Savart, Ann. Chim. **54**, 56 (1833).

[25] G. Taylor, Proc. R. Soc. A **253**, 296 (1959).

[26] F. E. C. Culick, J. Appl. Phys. **31**, 1128 (1960).

[27] C. Sohl, K. Miyano, and J. Ketterson, Rev. Sci. Instrum. **49**, 1464 (1978).

[28] A. Clarke, S. J. Weinstein, A. G. Moon, and E. A. Simister, Phys. Fluids **9**, 3637 (1997).

[29] W. W. Hagerty and J. Shea, J. Appl. Mech. **22**, 509 (1955).

[30] A. Mansour and N. Chigier, Phys. Fluids **3**, 2971 (1991).

[31] See Supplemental Material at http://link.aps.org/supplemental/10.1103/PhysRevLett.120.164501 for additional details. It is divided into five sections: I. Measurement of surface inclination angle, II. Additional Data, III. Scaling Analysis, IV. Theoretical predictions, V. Comparisons of the measurements with predictions of the aerodynamic theory, which includes Ref. [32].

[32] P. G. Drazin and W. Reid, *Hydrodynamic Stability* (Cambridge University Press, Cambridge, 1981), 1st ed.

[33] G. Crapper and N. Dombrowski, Int. J. Multiphase Flow **10**, 731 (1984).

[34] O. Tammisola, A. Sasaki, F. Lundell, M. Ma, and L. D. Soderberg, J. Fluid Mech. **672**, 5 (2011).

[35] J. Eggers, J. Fluid Mech. **672**, 1 (2011).

[36] J. B. Keller and I. Kolodner, J. Appl. Phys. **25**, 918 (1954).